View metadata, citation and similar papers at core.ac.uk

brought to you by CORE

東北大学機関リポジトリ
TOUR
Tohoku University Repository

Quantum Phase Transition in Itinerant-Electron Ferromagnet System U(Co1−xOsx)Al

著者	Mizuho Maeda, Alexander V Andreev, Kenji Shirasaki, Tomoo Yamamura, Noriaki Kimura
journal or publication title	Journal of the Physical Society of Japan
volume	87
number	9
page range	094713-1-094713-7
year	2018-08-29
URL	http://hdl.handle.net/10097/00126007

doi: 10.7566/JPSJ.87.094713

Quantum Phase Transition in Itinerant-Electron Ferromagnet System $U(Co_{1-x}Os_x)Al$

Mizuho Maeda[1*], Alexander V. Andreev[2], Kenji Shirasaki[3], Tomoo Yamamura[3], and Noriaki Kimura[1,4]

[1] *Department of Physics, Tohoku University, Sendai 980-8578, Japan*

[2] *Institute of Physics, Academy of Science, Na Slovance2, 182 21 Prague, Czech Republic*

[3] *Institute for Materials Research, Tohoku University, Sendai 980-8577, Japan*

[4] *Center for Low Temperature Science, Tohoku University, Sendai 980-8578, Japan*

We report the magnetic phase diagram of an itinerant-electron ferromagnetic system, $U(Co_{1-x}Os_x)Al$, derived from the AC susceptibility and DC magnetization. The quantum phase transition point at which the ferromagnetic transition temperature becomes 0 K is estimated to be located at $x \approx 0.004$. The tricritical point is also estimated to be located at $x \approx 0.0065$, $T \approx 11$ K. We also observed a non-Fermi liquid behavior near the quantum phase transition point: the temperature (T) dependence of the electrical resistivity (ρ) in the paramagnetic region is $\rho \propto T^{3/2}$ rather than $\rho \propto T^{5/3}$ that is predicted at the quantum critical point. The $T^{3/2}$ dependence is observed in some other itinerant-electron magnets, e.g., $ZrZn_2$ and MnSi. We discuss the possible mechanisms applied to these compounds.

1. Introduction

Quantum criticality is one of the most intriguing phenomena in solid state physics. Novel quantum states such as unconventional superconductivity,[1)] non-Fermi liquid (NFL) behavior,[2)] and exotic ordered states[3,4)] are often found near the border of magnetic order. In the itinerant-electron ferromagnetic system, the ferromagnetic state can often be suppressed by applying pressure. In many compounds, the ferromagnetic transition temperature T_C decreases with pressure and the transition changes from a continuous to a discontinuous (first-order) one at a tricritical point (TCP). With further pressure application, T_C becomes 0 K at P_c, corresponding to the quantum phase transition point (QPTP). In addition, the magnetic field (H) discontinuously induces a polarized (ferromagnetic) state, that is, a metamagnetic

*mmaeda@mail.clts.tohoku.ac.jp

transition starts to appear above the pressure of the TCP (P_{TCP}). The first-order metamagnetic transition ends at a critical temperature T_{cr} and changes to a crossover above T_{cr}.

This phase diagram is qualitatively explained by the theory considering the effect of spin fluctuations.[5,6] However, the nature of the quantum phase transition is still unclear. The self-consistent renormalization (SCR) theory predicts characteristic temperature (T) dependences in several physical quantities near the magnetic instability.[7] However, some itinerant-electron ferromagnetic compounds show a different temperature dependence. For example, the electrical resistivities (ρ) of $ZrZn_2$ and MnSi behave as $\rho \propto T^{3/2}$ just above P_{c}, although the SCR theory predicts $\rho \propto T^{5/3}$ at the quantum critical point (QCP).[8,9] This implies that the magnetic fluctuation in the vicinity of the QPTP is different from that at the QCP. To elucidate the physical nature of the QPTP, it is important to explore more examples. However, most examples need to apply high pressure to reach the QPTP,[10] which severely limits the experimental methods. Therefore, we focus on searching a substituted system that exhibits unusual spin fluctuations.

UCoAl with the hexagonal ZrNiAl-type crystal structure (space group $P\bar{6}2m$, No. 189) is one of the compounds exhibiting the above-mentioned T-H-P phase diagram.[11,12] At ambient pressure, UCoAl shows a metamagnetic transition at ≈ 0.6 T.[13] T_{cr} is ≈ 11 K and reaches 0 K under hydrostatic pressure. Although the ground state of UCoAl is paramagnetic, uniaxial pressure along the c-axis[14–16] or few percent of elemental substitution, such as Fe, Ru, and Os for Co, induces ferromagnetism.[17,18] Therefore, the QPTP can be reached by applying uniaxial pressure or changing the concentration x of the elemental substitution. Considering the relatively low metamagnetic transition field, UCoAl is considered to be close to the QPTP, which is an experimental advantage on investigating the nature of the QPTP. Indeed, the phase diagrams in the vicinity of the QPTP are revealed in $U(Co_{0.990}Ru_{0.010})Al$ and an isostructural compound URhAl by applying pressure.[19–21] The electrical resistivity is investigated for these compounds. In this paper, we focus on the recently composed $U(Co_{1-x}Os_x)Al$ system[22] and report a detailed T-H-x phase diagram and electrical resistivity at low temperatures down to 20 mK.

2. Experimental Procedure

Single crystals with the nominal composition $U(Co_{1-x}Os_x)Al$ (x = 0, 0.002, 0.005, 0.010, and 0.020) were grown by the Czochralski pulling method in a tetra-arc furnace. Except for $x = 0$, we obtained the samples from the same rods grown in a previous study.[22] The detailed procedure of the crystal growth of the Os-substituted samples

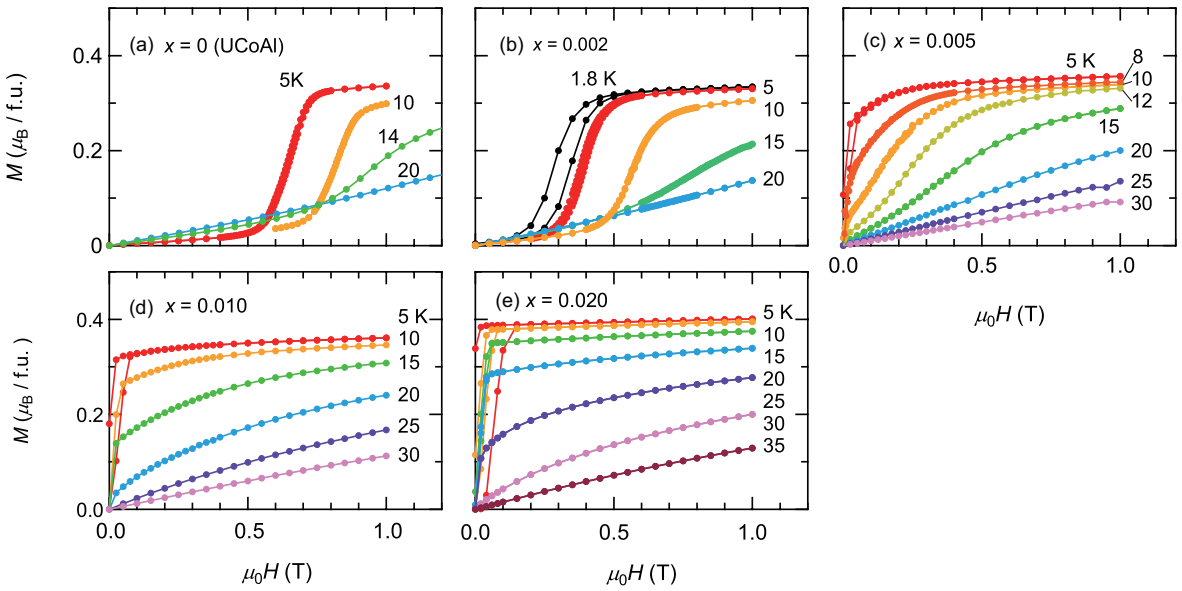

Fig. 1. (Color online) Magnetization curves of $U(Co_{1-x}Os_x)Al$.

is given in the literature. The obtained ingots were cut into rectangular shapes. The typical dimensions of the samples were approximately 1.0 (a-axis) × 3.0 (a^*-axis) × 1.0 (c-axis) mm^3 (about 30 mg mass). For UCoAl, the residual resistivity and its ratio were 16.4 $\mu\Omega$cm and 10, respectively, when the current I was applied along the hexagonal a^*-axis.

Static magnetization was measured using a Magnetic Property Measurement System (Quantum Design Inc.). The resistivity measurement down to 20 mK ($I//a^*$) was performed by a conventional four-probe method in a ^{4}He cryostat and a dilution refrigerator. AC susceptibility measurement was performed by a conventional mutual inductance method. A modulating field was superimposed on the static magnetic field. The frequency f and the amplitude h_0 of the modulating field were 23 Hz and 2 Oe in the sample for $x = 0.005$ and 23 Hz and 0.98 Oe in the others. A static magnetic field ($H//c$) was applied by a superconducting magnet. The effect of the remnant field of the superconducting magnet was corrected within an accuracy of 0.005 T. The demagnetization effect was omitted in all measurements.

3. Results and Discussion

3.1 Magnetization

The magnetization curves of $U(Co_{1-x}Os_x)Al$ are shown in Fig. 1. The results are in good agreement with previous reports.[12,18,22] The agreement suggests that the inhomogeneity of the Os composition in the single-crystal rods is negligible. For $x = 0$ and 0.002, the first-order metamagnetic transition was observed at low temperatures [Figs. 1(a) and 1(b)]. The

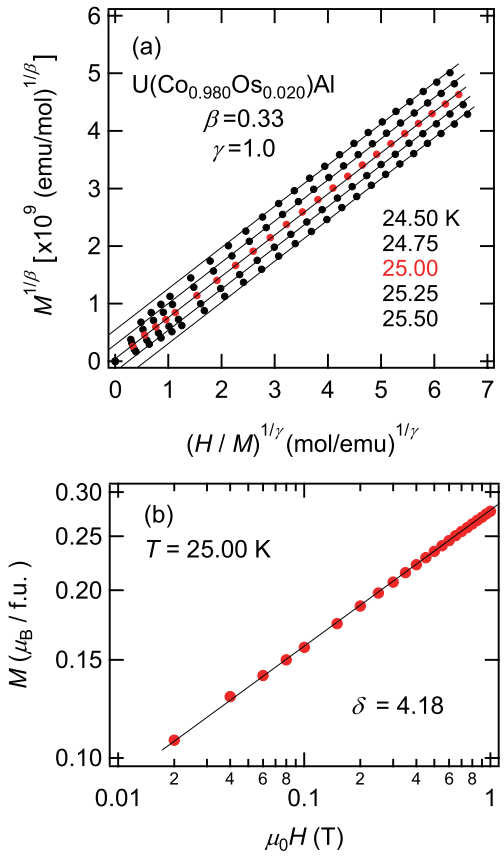

Fig. 2. (Color online) (a) Modified Arrott Plot and (b) determination of the critical index δ for $U(Co_{0.980}Os_{0.020})Al$. The lines are guides for the eyes.

transition clearly shows a hysteresis. With increasing temperature, the hysteresis disappears and the metamagnetic transition changes to a crossover. In general, it is difficult to determine the first-order transition point precisely when hysteresis exists. Here, we defined the metamagnetic transition field $H_{\rm m}^{M}$ as the midpoint of the peak fields in $dM_{\rm up}/dH$ and $dM_{\rm down}/dH$, where $M_{\rm up}$ and $M_{\rm down}$ are the magnetizations for increasing and decreasing the magnetic field, respectively. $H_{\rm m}^{M}(T)$ decreases with increasing x.

For $x \geq 0.005$, spontaneous magnetization was observed at low temperatures [Figs. 1(c)–1(e)]. Among these samples, the magnetization curves for $x = 0.005$ are different from a conventional ferromagnetic behavior; an "S"-shaped increase, indicating a transition or a crossover, exists in the temperature range of 8–18 K. Interestingly, the spontaneous magnetization and metamagnetic transition are successively observed at 8 and 10 K. At first sight, this seems to be inconsistent with the expected phase diagram mentioned in the introduction. However, such a magnetization curve is possible when the ferromagnetic transition is of the first order. The ferromagnetic phase coexists with the paramagnetic one in which the

metamagnetic transition occurs with increasing magnetic field. Although the hysteresis at the metamagnetic transition was not obvious in the DC magnetization curves, a finite energy loss due to the magnetic hysteresis is observed in the AC susceptibility, as will be shown later [Fig. 5(b)]. This hysteresis is evidence of the first-order nature of the ferromagnetic transition. The samples for $x = 0.010$ and 0.020 show a conventional ferromagnetic magnetization curve without a metamagnetic behavior [Figs. 1(d) and 1(e)].

From the magnetization data, we tried to determine T_C for the ferromagnetic samples ($x \geq 0.005$). However, the M^2 vs H/M plot (Arrott plot) for each sample was not linear, indicating that the mean-field approximation is not applicable to this system. Then, we applied the data to the so-called modified Arrott plot,[23] which can determine the critical indices β and γ in addition to T_C. The data for $x = 0.020$ exhibits a set of parallel lines in this plot, as seen in Fig. 2(a). $\beta = 0.33$, $\gamma = 1.0$, and $T_C = 25.00 \pm 0.02$ K are obtained for this sample. We also estimated the critical index δ from the log-log plot of $M(H)$ at T_C as shown in Fig. 2(b). The obtained $\delta = 4.18$ satisfies the scaling relation $\delta = 1 + \gamma/\beta$ within experimental error. These critical behaviors indicate that the ferromagnetic transition in $x = 0.020$ is not of the first order but of the continuous one.

The obtained combination of the critical indices is quite different from the well-known universality classes such as for the mean field model ($\beta = 0.5$, $\gamma = 1$, and $\delta = 3$) and that at the tricritical point ($\beta = 0.25$, $\gamma = 1$, and $\delta = 5$),[24] or for the 3D Ising model ($\beta \approx 0.33$, $\gamma \approx 1.24$, and $\delta \approx 4.79$).[25] γ in $x = 0.020$ corresponds to the mean field value, while those of β and δ support the 3D Ising model. Considering the strong magnetic anisotropy in this system, the 3D Ising type is favorable. The difference in γ may indicate that unusual critical fluctuations sensitively affect the magnetic susceptibility $\chi \sim (T - T_C)^{-\gamma}$. It is interesting to note that almost the same set of critical indices is obtained for UGe_2, which is an itinerant-electron ferromagnet ($T_C = 52$ K) at ambient pressure and can reach the TCP and QPTP with pressure application.[26]

Unlike in the case of $x = 0.020$, no combination of indices could make a set of parallel lines in the modified Arrott plot for $x = 0.005$ and 0.010. As for $x = 0.005$, the metamagnetic behavior of the magnetization is probably the main reason for the failure. A similar tendency, but less obvious, might also exist at $x = 0.010$.

3.2 AC susceptibility

AC susceptibility is a useful tool for the determination of the CP.[12] The real part χ' in a paramagnetic state gives the magnetic susceptibility dM/dH, while the imaginary part χ''

measures the energy loss due to the hysteresis of magnetization.

The results of the AC susceptibility measurements for $x \geq 0.002$ are shown in Figs. 3–5. The behaviors of χ' and χ'' for $x = 0.002$ were qualitatively the same as those for UCoAl.[12] We determined the metamagnetic CP using the same definition as Ref. 12: the point where $\chi''(T)$ vanishes and $\chi'(T)$ peaks. We obtained $(T_{\rm cr}, H_{\rm cr}) = (9.8 \pm 0.3$ K, 0.57 ± 0.04 T) for $x = 0.002$, which is indicated by white stars in Fig. 3.

The same definition of the critical point should be applicable to the ferromagnetic transition in principle. For $x = 0.020$, the peak temperature of $\chi'(T, 0\ {\rm T})$ is in good agreement with $T_{\rm C}$ determined from the modified Arrott plot (Fig. 4). However, χ'' does not disappear at $T_{\rm C}$ but remains at higher temperatures. The reason for the finite energy loss above $T_{\rm C}$ is not clear. For $x = 0.010$, since we could not determine $T_{\rm C}$ from the DC magnetization, we defined $T_{\rm C}$ as the peak temperature of $\chi'(T)$ and obtained $T_{\rm C} = 16.7 \pm 0.4$ K. The behaviors of χ' and χ'' for $x = 0.010$ are qualitatively the same as those for $x = 0.020$, suggesting that the ferromagnetic transition is still continuous. Both samples show shoulder structures in χ' and χ''. Because no anomaly was observed in the static magnetization at the corresponding temperature, this may be a specific property reflecting a dynamical magnetic behavior of these compounds. We note that a similar shoulder structure in χ' is also seen in the U($Co_{1-x}Ru_x$)Al system.[27] By applying a magnetic field, χ' and χ'' rapidly decrease as shown by the dashed lines in the figure.

The contour maps of the AC susceptibility for $x = 0.005$ are shown in Fig. 5. The metamagnetic transition field $H_{\rm m}^{\chi}$ is also plotted. Here, $H_{\rm m}^{\chi}$ is defined as the peak field of $\chi'(H)$. $H_{\rm m}^{\chi}$ mostly corresponds to $H_{\rm m}^{M}$. Apparently, χ' becomes maximum at a finite magnetic field and χ'' vanishes at the same point. These are signatures of a metamagnetic CP. We determined the location of the CP to be (11.1 ± 0.7 K, 0.20 ± 0.05 T) by the same definition mentioned above. The existence of the CP indicates that a first-order metamagnetic transition should occur below $T_{\rm cr}$. We estimated the metamagnetic transition line by fitting the data points of $H_{\rm m}^{\chi}$ by the equation $H_{\rm m}^{\chi} = a + bT^2$ (a, b : const.),[28] as shown in Fig. 5. As the extrapolated metamagnetic transition line crosses the T-axis, the ferromagnetic transition at 0 T should be of the first order. In this case, we cannot use χ' for the determination of $T_{\rm C}$. This is because the susceptibility does not diverge at the first-order ferromagnetic transition point owing to the coexistence of ferromagnetic and paramagnetic components.[29] We then defined $T_{\rm C}$ as the intersection of the metamagnetic transition line and the T-axis. The obtained $T_{\rm C}$ is 7.0 $\pm$ 0.6 K, which is lower than the peak temperature of $\chi'(T, 0\ {\rm T})$. A long tail of $\chi''(T, 0\ {\rm T})$ is also seen above 10 K. The coexistence region seems to extend to higher temperatures. Such a

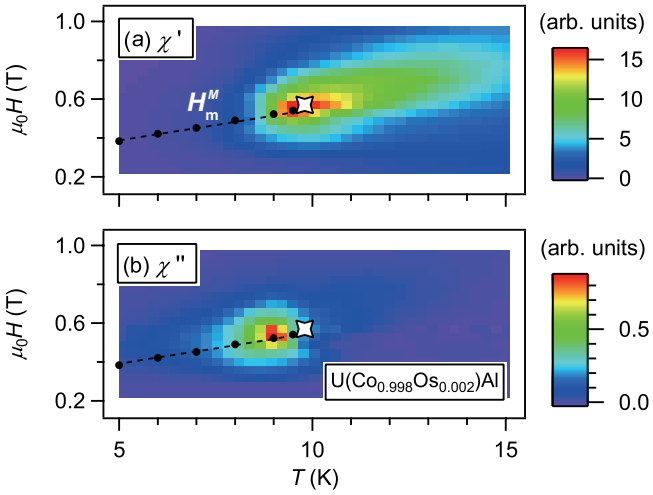

Fig. 3. (Color online) Color plots of the real part χ' and the imaginary part χ'' of the AC susceptibility for $U(Co_{0.998}Os_{0.002})Al$. The plots are constructed by interpolating the results of temperature sweeps at static fields. The white star indicates the metamagnetic critical point. The black dots represent H^M_m. The dashed lines are guides for the eyes.

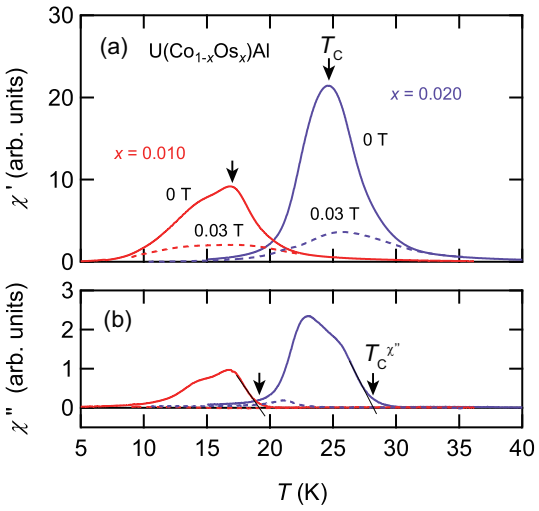

Fig. 4. (Color online) AC susceptibility of $U(Co_{1-x}Os_x)Al$ ($x = 0.010$ and 0.020) as a function of temperature. T_C is indicated by the arrows. Note that we cannot simply compare the amplitudes of the two Os concentrations because of the different shapes of the samples.

coexistence is microscopically confirmed by the ^{59}Co-NQR measurement in a similar system $U(Co_{0.980}Fe_{0.020})Al$.[30)]

We constructed the T-H-x phase diagram shown in Fig. 6 from the DC magnetization and AC susceptibility results. The obtained phase diagram is almost consistent with the schematic one previously determined by the DC magnetization.[22)] In this study, we determined continuous phase transition lines, indicated by the single lines in Fig. 6, more precisely owing to the

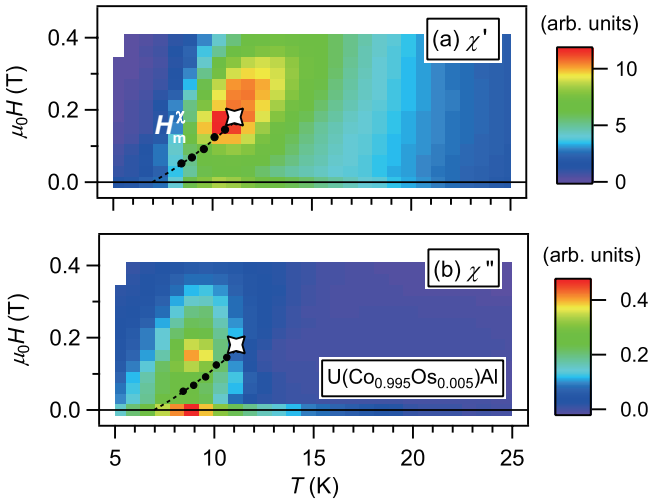

Fig. 5. (Color online) Color plots of the real part χ' and the imaginary part χ'' of the AC susceptibility for $U(Co_{0.995}Os_{0.005})Al$. The plots are constructed by interpolating the results of temperature sweeps at static fields. The white star indicates the metamagnetic critical point. The black dots represent H_m^{χ}. The dashed lines are fits to H_m^{χ} (see text).

AC susceptibility measurement. Since the metamagnetic transition is observed for $x = 0.005$ and is absent for $x = 0.010$, the TCP should be located within $0.005 < x < 0.010$. We estimated the location of TCP from the extrapolation of the critical field $H_{cr}(x)$ to the zero field (inset of Fig. 6). The estimated concentration x_{TCP} is 0.0065 and the corresponding transition temperature T_{TCP} is 11 K. The quantum phase transition point x_c, where T_C vanishes, locates within $0.002 < x_c < 0.005$. We estimated $x_c \approx 0.0035$ from a smooth extrapolation of $T_C(x)$.

3.3 Electrical resistivity

The temperature dependence of the electrical resistivity ρ is shown in Fig. 7. For $x = 0.010$ and 0.020, the resistivity shows a kink at T_C. For $x = 0.005$, on the other hand, the kink temperature ≈ 11 K is higher than $T_C \approx 7$ K determined from the DC magnetization. It corresponds rather to the peak temperature of $\chi'(T)$. This difference is again due to the ambiguity of T_C of the first-order transition. For $x \leq 0.002$, no drastic change in the slopes was observed down to the lowest temperature, suggesting the paramagnetic ground state of these samples.

Figure 8 shows the resistivity plotted against T^2. For the samples with the ferromagnetic ground state ($x \geq 0.005$), a linear dependence on T^2 is seen in a comparatively wide temperature range. In contrast, the linear region does not exist or is quite limited for the samples with the paramagnetic ground state ($x \leq 0.002$). By forcibly fitting the resistivities to the T^2 law,

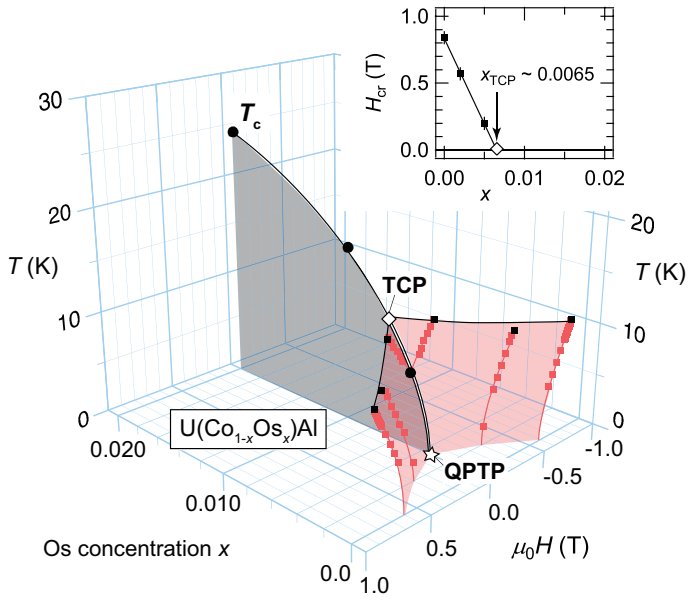

Fig. 6. (Color online) T-H-x phase diagram of U(Co$_{1-x}$Os$_x$)Al. The single and double black lines indicate continuous and discontinuous transitions, respectively. The red (light gray) planes indicate the metamagnetic transition planes. T_Cs for $x = 0.020$, 0.010, and 0.005, indicated by the closed circles, are determined from the modified Arrott plot, the peak of $\chi'(T)$, and the extrapolation of H_m^χ, respectively. The metamagnetic transition fields indicated by the red (gray) squares are determined from H_m^χ for $x = 0.005$, and from H_m^M for $x = 0$ and 0.002. The black squares indicate the CP of the metamagnetic transition. The data in $\mu_0 H < 0$ is mirrored from that in $\mu_0 H > 0$. (Inset) x dependence of the metamagnetic critical field H_{cr}. The line is fit to the data.

$\rho = \rho_0 + AT^2$, where ρ_0 and A are the residual resistivity and A coefficient, respectively, we obtain the T^2 region indicated as T^* in the T-x phase diagram (Fig. 9).

The x dependence of the A coefficient is shown in the inset of Fig. 8. The A coefficient at 0 T is enhanced from $x = 0$ towards x_c and abruptly decreases above x_c. A similar behavior of A is also reported in the pressure dependence of an isostructural ferromagnet URhAl and U(Co$_{0.990}$Ru$_{0.010}$)Al, whose magnetic order vanishes under pressure.[19,21] The A coefficient in the polarized (ferromagnetic) state is smaller than that at 0 T, probably indicating the difference in the density of states between the paramagnetic and induced ferromagnetic states.[31]

The behavior of the resistivity in the paramagnetic state ($x < x_c$) suggests a breakdown of the canonical Fermi liquid (FL) description in a wide temperature range. The non-T^2 dependence of the electrical resistivity is often observed near QCP, at which strong magnetic fluctuations affect the interaction between conduction electrons. According to the SCR theory, the exponent n in $\rho - \rho_0 \propto T^n$ should be 5/3 rather than 2 in the presence of the 3D

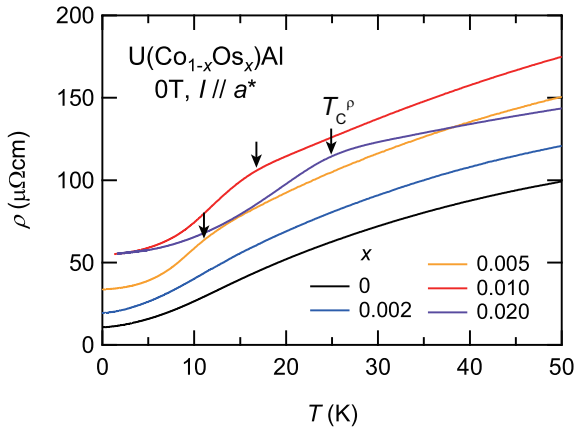

Fig. 7. (Color online) Electrical resistivity of $U(Co_{1-x}Os_x)Al$.

ferromagnetic fluctuation.[7] Indeed, $n \approx 5/3$ was previously reported for pure UCoAl.[12,32] However, as we have shown in Sect. 3.2, x_c is not a QCP but a QPTP since the transition at x_c is of the first order. Therefore, we should analyze the temperature dependence of the resistivity more carefully for $x \leqq x_c$.

Figure 10(a) shows resistivity as a function of $T^{5/3}$ below $\approx$ 6 K for $x = 0$ (pure UCoAl). A good linearity is seen at temperatures down to 1.7 K (= 2.4 $K^{5/3}$), which is consistent with a previous report.[32] However, the data at lower temperatures deviates from the line. Alternatively, the $T^{3/2}$ plot of the resistivity exhibits a better linearity than the $T^{5/3}$ plot down to the lowest temperature we measured, as shown in Fig. 10(b). The resistivity in $x = 0.002$ also behaves as $\rho \propto T^{3/2}$ in a slightly wider temperature range than that in UCoAl [Fig. 10(d)]. The $T^{3/2}$ region is indicated by T^{**} in the T-x phase diagram (Fig. 9).

4. Discussion

The $T^{3/2}$ dependence of the resistivity, namely, the NFL behavior, near the border of ferromagnetism is also observed in other materials, such as MnSi[8] and $ZrZn_2$,[9] as mentioned in the introduction. Ni_3Al is also reported to show the same temperature dependence.[33] In MnSi, the partial ordering of the conduction electron is revealed in the NFL region.[34] A $T^{3/2}$-law is theoretically introduced taking into account the possible columnar fluctuations of spin textures with the partial order of them,[35] and the relationship between the NFL behavior and topologically nontrivial spin vortices, namely, skyrmion, as the most plausible spin texture, is experimentally revealed.[4] The skyrmion lattice generally requires chirality in the crystal structure. However, the crystal structure of UCoAl is not chiral although it lacks an inversion center. Therefore, the NFL in $U(Co_{1-x}Os_x)Al$ cannot be explained by the same mechanism

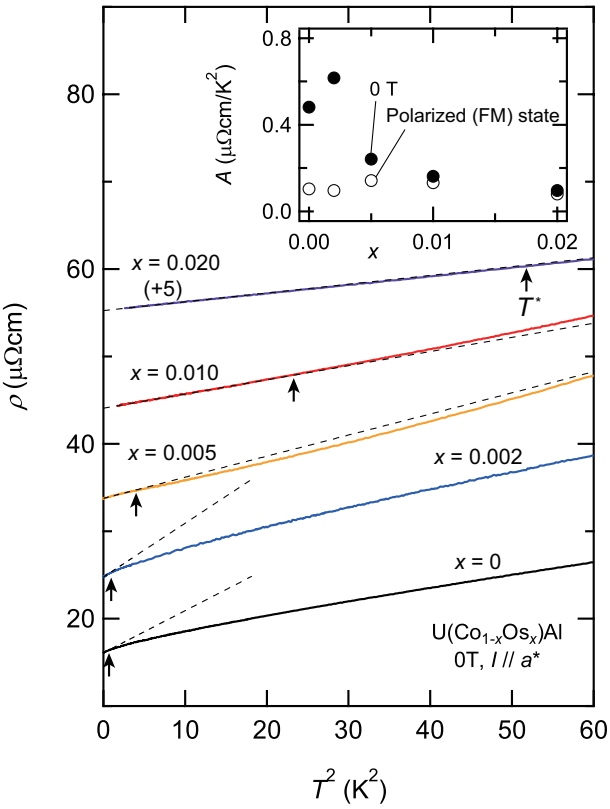

Fig. 8. (Color online) T^2 plots of the electrical resistivity in $U(Co_{1-x}Os_x)Al$. The dashed lines are fits to the data at 20 mK–0.55 K for x = 0–0.005 and 1.5–3 K for x = 0.010 and 0.020. The data for x = 0.020 is shifted upward by 5 $\mu\Omega$cm. (Inset) x dependence of A coefficient. The data for the induced ferromagnetic state were taken at 3.0 T for x = 0.002 and 1.5 T for the others.

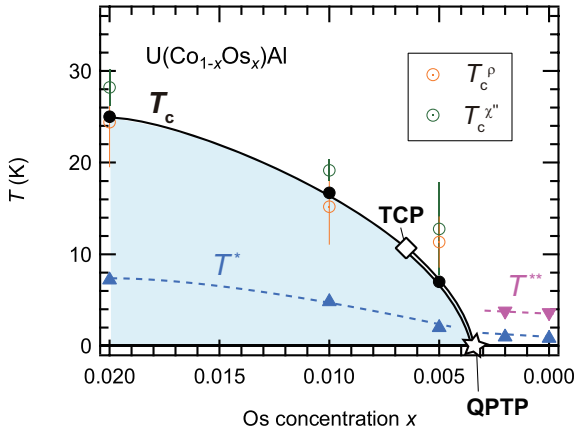

Fig. 9. (Color online) T-x phase diagram extracted from Fig. 6. The open circles indicate the kink temperature in the resistivity and onset of $\chi''(T)$ (see Figs. 7 and 4, respectively). The deviation temperatures from T^2 and $T^{3/2}$ dependences in the resistivity (T^* and T^{**}) are indicated by the closed triangles and inverted triangles (see Figs. 8 and 10), respectively.

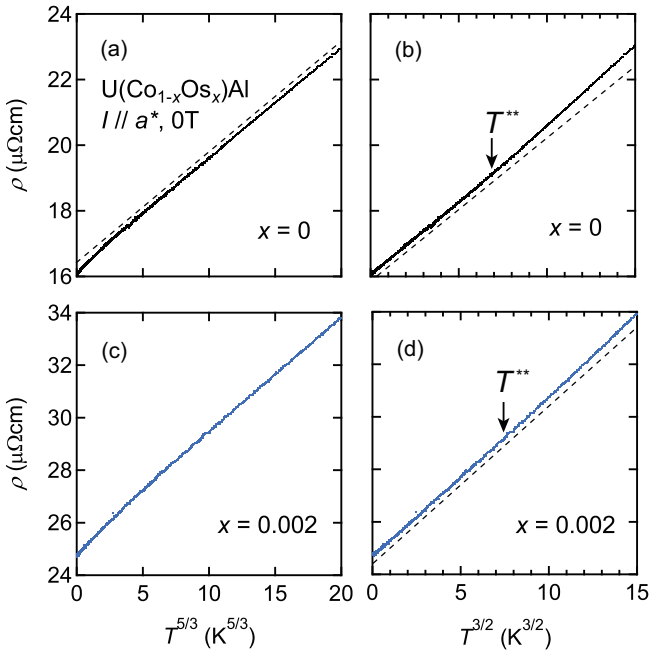

Fig. 10. (Color online) Electrical resistivities of $x = 0$ [(a) and (b)] and 0.002 [(c) and (d)] plotted against $T^{5/3}$ [(a) and (c)] and $T^{3/2}$ [(b) and (d)]. The dashed lines are fits to the data in the temperature ranges of 7–10 K [(a)] and 1–2 K [(b) and (d)]. The fitted lines are slightly shifted vertically for clarity.

proposed in MnSi.

As for $ZrZn_2$, the effect of antiferromagnetic fluctuation, which is theoretically predicted to cause $T^{3/2}$ dependence in the resistivity,[7] is discussed. The existence of the short-range antiferromagnetic ordering is deduced from the "negative" slope of the metamagnetic transition line in the H-T phase diagram and the nested Fermi surfaces.[36] However, in $U(Co_{1-x}Os_x)Al$, no signature of antiferromagnetism has been found thus far. Searching for an antiferromagnetic correlation might be interesting.

Recently, a $T^{3/2}$ behavior of the resistivity has been theoretically derived for ferromagnetic metals with weak disorder.[37] This can be applied to a partial ordering state of ferromagnetism possibly realized near the first-order transition line of the ferromagnetic phase. In such a state, the magnon-mediated scattering of electrons among exchange-split Fermi surfaces yields a peculiar temperature dependence of the scattering rate. To verify this scenario, the partial order of the ferromagnetic phase should be observed. Comparison with the temperature dependence away from the first-order transition line or the QPTP will also be useful. An application of pressure for UCoAl will be appropriate for the comparison. Unfortunately, however, the previous resistivity measurements of UCoAl under pressure[11,12] were insufficient to derive the precise temperature dependence at low temperatures. This issue is left for

further study.

A non-T^2 dependence in the paramagnetic phase near the QPTP is also observed in other isostructural compounds, e.g., $UCo_{0.95}Al_{1.05}$ at ambient pressure and URhAl and $U(Co_{0.990}Ru_{0.010})Al$ under pressure.[19,21,38] URhAl shows $n = 1.6$–1.7, which is close to $5/3$, while the other two compounds exhibit $n \approx 3/2$. The NFL ($n = 3/2$) behavior may be characteristic of the base compound UCoAl. Note that the $T^{3/2}$ dependences for $U(Co_{0.990}Ru_{0.010})Al$ under pressure ($T^{**} \approx 10$ K) are relatively wide in range compared with those of $U(Co_{0.998}Os_{0.002})Al$ and UCoAl ($T^{**} \approx 4$ K). The electrical resistivity in the paramagnetic state close to the QPTP may be sensitive to atomic composition or elemental substitution. According to the above-mentioned theory,[37] T^{**}, corresponding to T_0 in the literature, is associated with both band structure and magnon energy. The difference in T^{**} may be attributed to these properties.

As mentioned in Sect. 3.1, the critical indices of the ferromagnetic $x = 0.020$ are close to those of UGe_2. This resemblance suggests that a similar type of spin fluctuation is dominant at T_C for both compounds. In UGe_2, however, the FL behavior ($\rho - \rho_0 \propto T^2$) with a strong enhancement of the A coefficient is observed,[39] which is in sharp contrast to the present result. The quantum fluctuation in the $U(Co_{1-x}Os_x)Al$ system may be different from that in UGe_2.

5. Summary

We revealed the T-H-x phase diagram of $U(Co_{1-x}Os_x)Al$ by AC susceptibility and magnetization measurement. We also found a NFL behavior in the electrical resistivity near the QPTP. The temperature dependence of the electrical resistivity ρ well fits $T^{3/2}$ rather than $T^{5/3}$, which cannot be explained by the conventional SCR theory. Further research is desired in order to investigate the origin of the NFL behavior near the QPTP.

Acknowledgment

MM and NK would like to thank M. Kikuchi, H. Moriyama, and N. Fukiage for their technical support. This work was supported by JSPS KAKENHI Grant Numbers JP23654109 and JP26400345, and Grant Number 16-03593S of the Czech Science Foundation. This work was also performed under the Inter-University Cooperative Research Program of the Institute for Materials Research, Tohoku University (Proposal Numbers 16K0208 and 17K0201). AVA utilized the Materials Growth and Measurement Laboratory (https://mgml.eu).

References

1) F. Steglich, J. Aarts, C. D. Bredl, W. Lieke, D. Meschede, W. Frantz, and H. Schäfer, Phys. Rev. Lett. **43**, 1982 (1979).

2) G. R. Stewart, Rev. Mod. Phys. **73**, 797 (2001).

3) R. A. Borzi, S. A. Grigera, J. Farrell, R. S. Perry, S. J. S. Lister, S. L. Lee, D. A. Tennant, Y. Maeno, and A. P. Mackenzie, Science **315**, 214 (2007).

4) R. Ritz, M. Halder, M. Wagner, C. Franz, A. Bauer, and C. Pfleiderer, Nature **497**, 231 (2013).

5) H. Yamada, Phys. Rev. B **47**, 11211 (1993).

6) D. Belitz, T. R. Kirkpatrick, and T. Vojta, Phys. Rev. Lett. **82**, 4707 (1999).

7) T. Moriya: *Spin Fluctuations in Itinerant Electron Ferromagnetism* (Springer-Verlag, Berlin, 1985).

8) C. Pfleiderer, S. R. Julian, and G. G. Lonzarich, Nature **414**, 427 (2001).

9) S. Takashima, M. Nohara, H. Ueda, N. Takeshita, C. Terakura, F. Sakai, and H. Takagi, J. Phys. Soc. Jpn. **76**, 043704 (2007).

10) M. Brando, D. Belitz, F. M. Grosche, and T. R. Kirkpatrick, Rev. Mod. Phys. **88**, 025006 (2016).

11) D. Aoki, T. Combier, V. Taufour, T. D. Matsuda, G. Knebel, H. Kotegawa, and J. Flouquet, J. Phys. Soc. Jpn. **80**, 094711 (2011).

12) N. Kimura, N. Kabeya, H. Aoki, K. Ohyama, M. Maeda, H. Fujii, M. Kogure, T. Asai, T. Komatsubara, T. Yamamura, and I. Satoh, Phys. Rev. B **92**, 035106 (2015).

13) V. Sechovský, L. Havela, F. R. de Boer, J. J. M. Franse, P. A. Veenhuizen, J. Sebek, J. Stehno, and A.V. Andreev, Physica B **142**, 283 (1986).

14) Y. Ishi, M. Shiokawa, Y. Uwatoko, A.V. Andreev, and V. Sechovský, Physica B **334**, 160 (2003).

15) K. Karube, S. Kitagawa, T. Hattori, K. Ishida, N. Kimura, and T. Komatsubara, J. Phys. Soc. Jpn. **83**, 084706 (2014).

16) Y. Shimizu, B. Salce, T. Combier, D. Aoki, and J. Flouquet, J. Phys. Soc. Jpn. **84**, 023704 (2015).

17) A. V. Andreev, H. Atuga Karoti, and T. Goto, J. Alloys Compd. **22**, 117-120 (1995).

18) A. V. Andreev, K. Shirasaki, J. Šebek , J. Vejpravová, D. I. Gorbunov, L. Havela, S. Daniš, and T. Yamamura, J. Alloys Compd. **681**, 275 (2016).

19) P. Opletal, J. Prokleška, J. Valenta, P. Proschek, V. Tkáč, R. Tarasenko, M. Béhounková, S. Matoušková, M. M. Abd-Elmeguid, and V. Sechovský, npj Quantum Materials **2**, 29 (2017).

20) P. Opletal, J. Prokleška, J. Valenta, and V. Sechovský, AIP Advances **8**, 055710 (2018).

21) Y. Shimizu, D. Braithwaite, B. Salce, T. Combier, D. Aoki, E. N. Hering, S. M. Ramos, and J. Flouquet, Phys. Rev. B **91**, 125115 (2015).

22) A. V. Andreev, J. Šebek, K. Shirasaki, S. Daniš, D. I. Gorbunov, T. Yamamura, J. Vejpravová, L. Havela, and F. R. de Boer, Physica B **536**, 558 (2018).

23) A. Arrott and J. E. Noakes, Phys. Rev. Lett. **19**, 786 (1967).

24) P. M. Chaikin and T. C. Lubensky, *Principles of Condensed Matter Physics* (Cambridge University Press, Cambridge, 1995) Chap. 4.

25) H. W. J. Blöte, E. Luijten, and J. Heringa, J. Phys. A **28**, 6289 (1995).

26) N. Tateiwa, Y. Haga, T. D. Matsuda, E. Yamamoto, and Z. Fisk, Phys. Rev. B **89**, 064420 (2014).

27) J. Pospíšil, P. Opletal, M. Vališka, Y. Tokunaga, A. Stunault, Y. Haga, N. Tateiwa, B. Gillon, F. Honda, T. Yamamura, V. Nižňanský, E. Yamamoto, and D. Aoki, J. Phys. Soc. Jpn. **85**, 034710 (2016).

28) N. Mushnikov, T. Goto, K. Kamishima, H. Yamada, A. V. Andreev, Y. Shiokawa, A. Iwao, and V. Sechovský, Phys. Rev. B **59**, 6877 (1999).

29) T. R. Kirkpatrick and D. Belitz, Phys. Rev. B **93**, 144203 (2016).

30) K. Karube, T. Hattori, K. Ishida, and N. Kimura, Phys. Rev. B **91**, 075131 (2015).

31) T. D. Matsuda, Y. Aoki, H. Sugawara, H. Sato, A. V. Andreev, and V. Sechovský, J. Phys. Soc. Jpn. **68**, 3922 (1999).

32) L. Havela, M. Diviš, V. Sechovský, A.V. Andreev, F. Honda, G. Oomi, Y. Meresse, and S. Heathman, J. Alloys Compd. **322**, 7-13 (2001).

33) P. G. Niklowitz, F. Beckers, G. G. Lonzarich, G. Knebel, B. Salce, J. Thomasson, N. Bernhoeft, D. Braithwaite, and J. Flouquet, Phys. Rev. B **72**, 024424 (2005).

34) C. Pfleiderer, D. Reznik, L. Pintschovius, H. v. Löhneysen, M. Garst, and A. Rosch, Nature **427**, 227 (2004).

35) T. R. Kirkpatrick and D. Belitz, Phys. Rev. Lett. **104**, 256404 (2010).

36) N. Kabeya, H. Maekawa, K. Deguchi, N. Kimura, H. Aoki, and N. K. Sato, J. Phys. Soc. Jpn. **81**, 073706 (2012).

37) T. Kirkpatrick and D. Belitz, Phys. Rev. B **97**, 064411 (2018).

38) A. V. Kolomiets, L. Havela, V. Sechovský, L. E. DeLong, D. B. Watkins, and A. V. Andreev, J. Appl. Phys. **83**, 6435 (1998).

39) T. Terashima, K. Enomoto, T. Konoike, T. Matsumoto, S. Uji, N. Kimura, M. Endo, T. Komatsubara, H. Aoki, and K. Maezawa, Phys. Rev. B **73**, 140406 (R) (2006).